Environ Monit Assess
DOI 10.1007/s10661-008-0577-y

Shadow attenuation with high dynamic range images

Creating RGB images that allow feature classification in areas otherwise obscured by shadow or oversaturation

Samuel E. Cox · D. Terrance Booth

Received: 8 July 2008 / Accepted: 22 September 2008

Abstract Shadow often interferes with accurate image analysis. To mitigate shadow effects in near-earth imagery (2 m above ground level), we created high dynamic range (HDR) nadir images and used them to measure grassland ground cover. HDR composites were created by merging three differentially exposed images spanning a wide exposure range and resulted in lightened shadows. HDR images showed more detail; reduced the numbers of pure black, pure white, and pixels visually indistinguishable from black and white; reapportioned skewed luma values towards a normal distribution; and increased the Euclidean distance between litter and bare ground RGB values—allowing increased feature separation; all of which facilitated an increase in real feature classification through manual image analysis. Drawbacks to the method included decreased image sharpness due to minor misalignment of images or moving vegetation, time required to create HDR images, and difficulty with acquiring primary images from a moving platform. We conclude that HDR imagery can provide more accurate measurements of bare soil cover for ecosystem monitoring and assessment.

Keywords Vegetation · Monitoring · Luma · Image analysis · Oversaturation · Underexposure

S. E. Cox (✉) · D. T. Booth
Agricultural Science Technician and Rangeland Scientist, USDA Agricultural Research Service, High Plains Grasslands Research Station, 8408 Hildreth Rd, Cheyenne, WY, 82009, USA
e-mail: Samuel.Cox@ars.usda.gov

Introduction

Image analysis as it relates to natural resource remote sensing is the process of extracting information from images obtained from satellite, aerial, or near-earth platforms. Whether the analysis uses pixel color or object shape and texture, shadows in the image hinder accurate image analysis by preventing assessment of all pixels, or by causing dissimilar features to have similar spectral radiance if both are shaded and by resulting in the same feature having dissimilar spectral radiance between shaded and unshaded areas (Booth and Tueller 2003). Naesset (1998) reported errors in commercial forest stand delineation from aerial photographs due to shadows cast by the trees. Nakashizuka et al. (1995) and Fujita et al. (2003) both reported reduced forest-canopy gap detection from aerial imagery due to shadows cast by trees. Anderson et al. (1996) reported reduced detection of leafy spurge in aerial imagery due to shadow in riparian areas cast by trees and shrubs. Bowman et al. (2001) reported that vegetation shadows hindered canopy-density mea-

surements from aerial images. Wittmann et al. (2002) reported that cloud shadows hampered forest species analysis of aerial images. Sawaya et al. (2003) reported that shadows reduced the accuracy of lake water clarity assessment and impervious surface area measurement from satellite imagery in hydrologic studies. To avoid shadows and provide uniform lighting, Bennett et al. (2000) used a cloth screen to shade plots during photography from 2 m above ground level. Standard remote sensing acquisition is regularly scheduled for midday to reduce shadows (Clemmer 2001; Everitt et al. 2001; Paruelo et al. 2000), although light aircraft platforms (such as Booth and Cox 2006) often schedule flights during morning hours to avoid high winds and convective turbulence, thereby increasing shadowed areas in imagery. Additional examples of shadow impacts are not hard to find. The problem becomes more acute at finer spatial resolutions where shadows from features like grass blades become apparent.

We have promoted the shading of photo plots in near-earth remote sensing to prevent deep shadows or bright washouts, but in high-wind, this is often impractical or requires two technicians (Booth et al. 2004). Typical outdoor, unshaded, high-contrast scenes can cover 10 stops of the camera's aperture; that is, correctly exposing for shadows requires an aperture setting 10 stops lower (larger) than correctly exposing for highlights such as rocks or sandy soil. Although the cutoff is gradual and defined by subjective image examination and thus variable, most photographic experts agree that transparency film cannot capture more than ~5 stops of contrast, negative film ~7 and fine-grained black and white film ~8 (Lodriguss 2003). Essentially, this is a description of dynamic range, which is defined as the log of the ratio of light intercepted by the sensor to the amount of light recorded by the sensor. Higher dynamic range yields more detail in dark and light areas. As portions of an image approach and exceed the dynamic range of the medium, details are either completely obscured by underexposure (black) or overexposure (white). High-end digital single lens reflex (SLR) cameras can only capture ~6–8 stops of contrast (Brown 2006), limited not just by lack of detail in dark and saturated areas but by the amount of digital noise resulting from increased gain (sensitivity) that makes details in dark areas virtually impossible to decipher. This means that no camera currently available can fully capture details of a high-contrast outdoor scene in a single exposure. This limitation can be overcome by capturing multiple images of the same field-of-view with varying shutter speeds at a constant aperture such that, for example, one image correctly exposes dark areas, another correctly exposes bright areas, and a third correctly exposes the areas in between. Manual and semi-automated processes and software allow merging multiple digital images into a single image to present scenes which can effectively span 10+ stops of contrast (depending on the number and exposure of images merged together) and thus have a higher dynamic range than normal imagery. These high dynamic range (HDR) images allow simultaneous examination of very dark and very bright areas within the same image, without loss of detail at the extremes of exposure or introduction of digital noise. Here we demonstrate the utilization of high dynamic range imagery for near-earth remote sensing in a grassland ecosystem and discuss the application of HDR imagery in aerial remote sensing.

Materials and methods

A Canon[1] 5D 12.8-megapixel digital SLR camera with 28–90 mm f/4.0–5.6 lens was mounted on a 2-m-tall aluminum camera frame with a 1-m^2 base and set to a focal length of 38 mm such that 0.8-mm ground sample distance nadir images were acquired from 2 m above ground level (Booth et al. 2004). Camera operation in auto-bracket mode resulted in capture of three RAW-format images of varying exposure for every station: normal, two stops underexposure, and two stops overexposure. Aperture-priority mode (f/8) was used so that the exposure varied only by shutter speed, thus keeping the relatively high depth of field constant across all bracketed images. Digital International Standards Organization (ISO) speed (gain) was set to 200. Twenty-five 1 m^2 plots were

[1]Mention of trade names or commercial products is for information only and does not imply recommendation or endorsement by the US Department of Agriculture.

systematically photographed in this manner on a sunny morning in early fall with sun angle of ~30° at the High Plains Grasslands Research Station, Cheyenne, WY, USA. The study area was characterized by perennial grasses and forbs on Nucla Loam soils (Stevenson et al. 1984) with low slope. RAW images of the normal (uncompensated) exposure for each plot were converted to TIF images. RAW images were also used to batch-create HDR images with Photomatix Pro 2.4 (HDR Soft, Montpellier, France) by combining each set of three images/plot into a single HDR file, then applying tone mapping to create a TIF image that drew detail from all three. Resulting HDR images were saved as 8-bit/channel (24 bit) TIF files and were largely free of areas that were too dark or too bright. Photomatix allows creation of 16-bit/channel imagery (48 bit), which may be of value if using analysis software that can handle 48-bit images; however, any software relying on visual inspection or analysis of imagery cannot benefit from 48-bit imagery because there exists no monitor technology to display anything higher than 24-bit imagery (Brown 2006). Thus, for manual analysis, such as this study used, there is no benefit to be gained from using 48-bit imagery. Both normal and HDR images were cropped to the size of the 1 m^2 plot frame, resulting in 2,500 × 2,500-pixel images used for testing.

Digital image color is typically defined by combinations of red, green and blue (RGB), each on a scale of 0 to 255. Luminance is a measure of the amount of emitted light, whereas brightness is a measure of the amount of light striking a defined area. Because digital media, such as computer monitors, have limits to how dark and how bright each pixel can be displayed, the perceived brightness of a pixel is constrained by the hardware (Poynton 1996). Coding brightness of real-world colors to fit within this constrained framework has resulted in a nonlinear, or gamma-compressed, color-band coding. Gamma-compressed luminance becomes luma, calculated using a set of standardized correction coefficients, as follows (from Poynton 1996):

$$\text{Luma } (Y') = 0.299R' + 0.587G' + 0.114B' \quad (1)$$

where R' = gamma-compressed red band value, G' = gamma-compressed green band value and B' = gamma-compressed blue band value. If shown three equal intensities of color: red, green, and blue, humans perceive green as brighter than red, and red brighter than blue (Poynton 1996). To compensate for this physiological feature of the human eye, coefficients are added to the luma equation to weight the primary colors based on an international standard (Rec. 601), thus giving digital images high-fidelity color (Poynton 1996).

Image luma histograms were generated and qualitatively examined using Photoshop Elements 2.0 (Adobe, San Jose, CA, USA). The number of completely black (RGB = 0, 0, 0) and completely white (RGB = 255, 255, 255) pixels were counted in every image using a program written in the C# programming language. Accuracy of the program was confirmed using blocks of known pixel quantity and RGB color generated in Photoshop Elements. Additionally, the number of image pixels with a luma of less than or greater than the median user-classified "shadow" and "saturated" values, respectively (derived from manual image analysis, explained below), were measured from each of the 25 images and compared between image type with paired *t* tests (Microsoft Excel 2003, Redmond, WA, USA).

Image pixel color can be plotted in a 3-dimensional space with axes: red, green and blue, so one can picture pixel color values of a relatively homogenous feature, such as bare ground, represented as a "cloud" within this 3-dimensional, cubic color space, a cloud whose size decreases with increasing feature-color homogeneity. Bare ground is a key indicator used to assess rangeland condition, but using color to measure bare ground is often confounded by the presence of similarly colored litter (Booth et al. 2005). In other words, the "cloud" of bare ground color values is often intermingled with the "cloud" of litter color values within the 3-dimensional color space, making it impossible to tell them apart based on color. To test the hypothesis that HDR imagery, by virtue of improving the color saturation in shadowed and oversaturated areas, would improve separation of these "clouds" of color values and thus improve the ability to separate bare ground from litter based on color, we analyzed RGB values for 10 bare and 10 litter pixels/image, randomly chosen from both normal and HDR images from

19 plots using multi-response permutation procedures (MRPP) (PC-ORD 4.01, MjM Software, Gleneden Beach, OR, USA). MRPP is a nonparametric procedure used for testing a hypothesis of no difference between two or more groups (Biondini et al. 1988). We used MRPP to compare the Euclidean distance of pixels in a 3-dimensional RGB color space within each of the two cover types (bare ground and litter) with the distance among all possible pairs of points. Specifically, the average distance between the 10 bare ground pixels (plotted in the 3-dimensional color space) from one image was compared with the average distance between all 20 pixels (both litter and bare ground) from that same image. Groups with significant spatial distance from each other within the 3-dimensional color space will have a lower within-group mean distance relative to the population mean distance, since they are closer to each other than to points in the overall population (Biondini et al. 1988). This separation between bare ground and litter pixel values is summarized by a chance-corrected within-group agreement statistic (A) provided by the MRPP analysis. A equals 0, when the heterogeneity within groups is equal to that expected by chance, and 1, when all points within a cover type have equal RGB values. We predicted that the separation between bare ground and litter should be greater in HDR imagery relative to normal imagery, manifested by a higher A statistic.

SamplePoint 1.37 (Booth et al. 2006) was used to manually measure cover from both the normal and HDR images by means of manual classification of 100 points/image in order to test the hypothesis that HDR images allow cover information to be extracted from areas that are too dark or bright to analyze in a normal image. SamplePoint classification categories included green grass, brown grass, forb, litter, bare ground, rock, shadow, saturated, and unknown. Green and brown grass classes are self-explanatory. Litter included detached and decomposing (gray) organic material and other unidentifiable organic matter in contact with the soil. The forb category included green and brown broadleaf plants. Only mineral soil was classified as bare ground. The shadow category included points that fell in areas too dark to be reasonably confident of manual classification. The saturated category included points where the complete light saturation of the area prevented reasonable confidence in classification. If a point could not be classified with reasonable confidence for reasons *other* than over- or underexposure, then that point was simply classified as unknown. The 50-image set was analyzed by five individuals using SamplePoint, each of whom were given the above written classification category definitions. HDR images were compared with normal images for differences in cover values influenced by the attenuation of shadow in the imagery using two-way analysis of variance (SAS v 9.1, SAS Institute, Nashville, TN, USA) for comparisons across all users and by t tests for comparisons among individual users.

Results and discussion

HDR imagery from a near-earth platform

Visually, HDR images present a much easier image to classify because bright and dark extremes, those areas that are too dark or light to allow discernment of detail or color, have been removed (Fig. 1). The human eye is very adept at rapidly adjusting the iris to examine dark and bright areas within a plot frame in the field, to the point where such extreme differences in light exposure go almost unnoticed. Images "fix" the exposure, thus removing from the equation the eye's ability to rapidly adjust to varied light. Instead of the eye doing the work, the HDR image effectively makes that adjustment for us, reducing the overall contrast of the image and compressing the detail into the constraints of an image that can be displayed on a typical computer monitor.

Both manual and automated classification techniques utilize color to some degree, with some methods relying on it exclusively, such as ERDAS Imagine (Leica Geosystems, Norcross, GA, USA) or VegMeasure (Johnson et al. 2003). Pixels whose RGB combinations are 0, 0, 0 (black) or 255, 255, 255 (white) confound classification because they are essentially wild cards hiding in the darkest and lightest classes. For example, a black pixel could be shadowed grass, shadowed forb or shadowed litter, but there is no way to tell exactly

Fig. 1 Normal (uncompensated) exposure of a 1 m^2 plot from 2 m above ground level (*left*), with a high dynamic range image of the same plot (*right*) showing increased detail in shadowed areas and less oversaturation in bright areas

what it is because the pixel itself conveys no useful spectral information. Purely black or white pixels represent inherent classification errors. HDR images displayed 1.8% fewer purely black or white pixels relative to normal images ($P < 0.001$, $n = 25$), resulting in more pixels/image with potential for meaningful classification (Table 1). For manual analysis, not only pure black and white pixels but even very dark and very bright pixels confound classification since pure black (0, 0, 0) is the same as "almost-black" (0, 15, 0) to the human eye. From manual image analysis, median luma values for all pixels classified as shadow or saturated were calculated as 24 and 234, respectively. Every human eye is different, but pixels with luma above 234 or below 24 are so visually close to white and black, respectively, that we feel very few people would be able to distinguish color from pixels with a luma of less than 24 or greater than 234, a conclusion that is supported by research findings from a limited number of users. These pixels will simply appear black or white. Relative to normal images, the number of pixels with luma above and below these median values was 33% lower in HDR images ($P < 0.001$), resulting in more pixels/image with potential for meaningful classification (Table 1). For our test images, this represents an average increase of 1.9 million pixels per image moving from essentially a "no-data" spectral signature to a classifiable spectral signature, an increase that is visually apparent (Fig. 1) and largely explains

Table 1 Mean amount ± SD of black and white, and nearly black and white, pixels from 25 normal and 25 high-dynamic range images of the same plots, expressed as a percentage of total image pixels, and the difference between them

	Normal	HDR	Difference
Pure black	0.5 ± 0.39	$5.3e^{-5} \pm 1.1e^{-4}$	0.5 ± 0.4
Pure white	1.4 ± 0.69	0.1 ± 0.05	1.3 ± 0.7
Luma ≤24	19.6 ± 6.7	0.002 ± 0.001	19.6 ± 6.7
Luma ≥234	13.8 ± 5.8	$7.4e^{-4} \pm 0.001$	13.8 ± 5.8

Approximately 6 million pixels were measured for each image. Luma cutoff values for dark and bright pixels are the median values for pixels manually classified as shadow (24) or saturated (234). All differences are significant $P < 0.001$

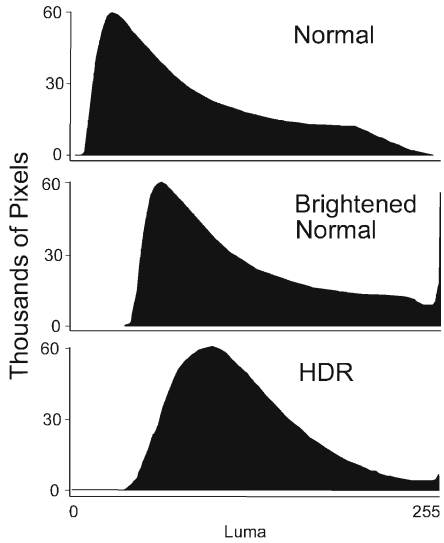

Fig. 2 Luma histograms of a randomly selected normal image from the study set shown for the normal exposure, the brightened normal image, and a high-dynamic range (*HDR*) image generated from the normal image plus two additional images with different exposure lengths (+0.05 s, −0.02 s shutter)

differences in manual classification between HDR and normal imagery described below.

From the histogram of a randomly selected normal image, pixel luma was skewed heavily towards low luma, with a mean luma of 86 (Fig. 2). Brightening the image in Photoshop increased the mean luma to 119, but retained the skewed distribution of pixel luma towards the low end. Brightening simply added value to every band at every pixel so that the histogram shape was retained but shifted towards higher luma. This resulted in a complete removal of all pixels in the lower fifth of the luma scale, whereas on the high end, pixels stacked up against the 255 (white) limit imposed by the RGB color model, resulting in a large increase in the number of completely saturated pixels with RGB values of 255. Pixels at or near the saturation level also hinder feature classification. Thus, while brightening an image may reduce deleterious shadow effects, it simultaneously increases deleterious saturation effects and is therefore not an ideal solution for correcting heavily shadowed imagery. The associated HDR image had a mean luma of 119, as in the brightened image, but much of the skew towards low luma was removed so that luma values approached a normal distribution with a higher median luma value (Fig. 2). While most dark pixels in the lower fifth of the scale have been removed, some remain, and while there are more saturated pixels in the HDR image relative to the normal image, there

Table 2 Results from multi-response permutation procedures comparisons of bare ground and litter color within normal and HDR images of each 1 m^2 plot

A higher *A* statistic indicates a larger difference between bare ground and litter pixel color in the randomly selected pixels for each cover class within each plot. HDR imagery showed greater pixel color separation between bare ground and litter in 63% of the plots

Plot	*A* Statistic		
	Normal	HDR	Type with higher separability
1	−0.01	0.31	HDR
2	0.16	−0.01	Normal
3	0.76	0.08	Normal
4	0.18	0.26	HDR
5	0.17	0.01	Normal
6	0.04	0.15	HDR
7	0.29	0.4	HDR
8	0.37	0.01	Normal
9	0.15	0.37	HDR
10	0.05	0.28	HDR
11	0.04	0.46	HDR
12	0.49	0.31	Normal
13	0.01	0.05	HDR
14	0.14	0.26	HDR
15	−0.01	0.02	HDR
16	0.07	0.11	HDR
17	0.38	0.34	Normal
18	0.31	0.51	HDR
19	0.38	0.02	Normal

are far fewer than in the brightened image. This translates into an HDR image with more pixels in the luma mid-range and fewer pixels in the upper and lower fifths of the luma scale, resulting in an image that is easier for the human eye to analyze, thus leading to quicker and easier manual feature classification.

MRPP analyses showed that across all 19 plots, HDR images allowed for greater separation between litter and bare ground color relative to the normal images, even when both showed significant separation, in 12 of 19 comparisons (Table 2). In other words, for 63% of the photos analyzed, bare ground color was more distinct from litter color in HDR images. This establishes that bare ground and litter ought to be more separable in HDR images than in normal images, whether classification is performed manually or using automated software, although the result is not universal, and it must be noted that normal images outperformed HDR images in this respect 37% of the time. Based on this evidence alone, it would be difficult to make a case for using HDR images in analysis; however, as a piece of evidence among many, it helps to support HDR image use.

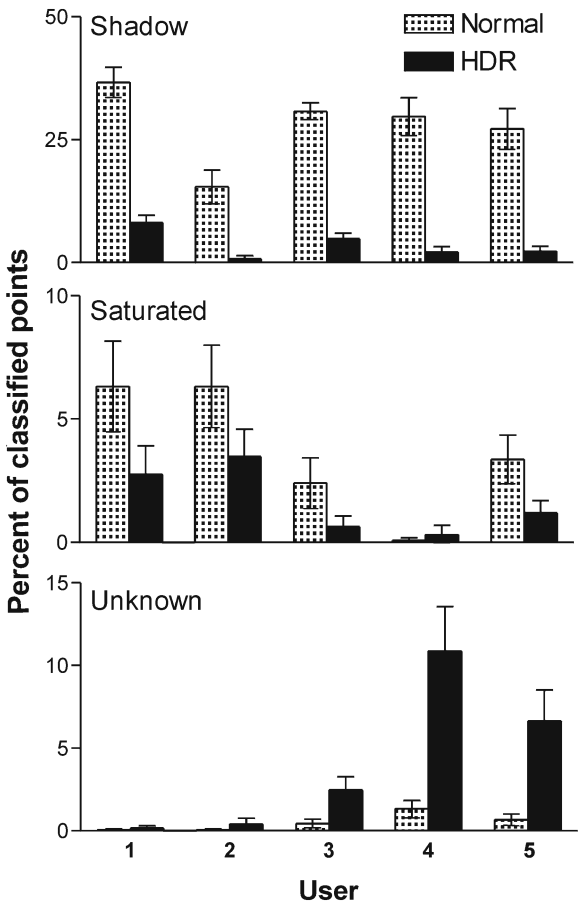

Fig. 3 Percent manual classification points classified as shadow, saturated, or unknown across all five users for normal and high dynamic range images of 25 plots. *Error bars* represent 95% confidence interval of the mean

Manual image analysis revealed that merging several images into a single HDR image for analysis significantly changed cover measurements. On an individual user basis relative to the normal imagery, the number of points classified as shadow was always lower in HDR images, and the number of points classified as saturated was usually lower when classifying HDR images (Fig. 3). Across all users, shadow decreased 24.3% ± 8.3 SD, and saturated points decreased 2.0% ± 3.0 SD with HDR classification ($P < 0.001$, $n = 5$ users); however, the effects for some cover classes were dependant on the user, as seen in significant interaction between user and image type (Table 3). The 26% reduction in the number of points that could not be classified because of darkness/brightness resulted in increases of measured green grass (7.7% ± 3.7 SD), brown grass (3.6% ± 5.0 SD), litter (5.7% ± 6.1 SD), rock (0.5% ± 0.9 SD), and bare ground (5.0% ± 6.2 SD) ($P < 0.05$, Fig. 4). User interaction with image type was not significant ($P > 0.05$) for traditional life form classes but was significant for three classes: shadow, saturated, and unknown, classes that are more subjective than life form classes. Although every user was presented with the same set of instructions for classification, shadow and saturated category classification showed significant user interaction attributable to a single user in each case (Table 3). Removing the outlying user eliminated significant treatment × user interaction for the shadow and saturated categories (Table 3), although that is not to discount that such variation among users exists as a factor that is likely to be encountered with manual image analysis. This suggests that either some users interpreted the written definitions of shadow and saturated differently or that varying

Table 3 Significance probability values from a two-way analysis of variance that measured the effect of HDR image enhancement against normal images (treatment), and user effects (user)

Class	Treatment	User	Interaction	Difference	Interaction with anomalous user data removed
Green grass	< 0.0001	0.013	0.7928	7.7 ± 3.7	–
Brown grass	0.0024	0.0012	0.0527	3.6 ± 5.0	–
Forb	0.8763	0.0002	0.9997	–	–
Litter	< 0.0001	< 0.0001	0.0979	5.7 ± 6.1	–
Rock	0.0251	< 0.0001	0.5299	0.5 ± 0.9	–
Bare ground	< 0.0001	< 0.0001	0.1592	5.0 ± 6.2	–
Shadow	< 0.0001	< 0.0001	< 0.0001	−24.3 ± 8.3	0.45
Saturated	< 0.0001	< 0.0001	0.0046	−2.0 ± 3.0	0.41
Unknown	< 0.0001	< 0.0001	< 0.0001	3.6 ± 4.6	< 0.0001

The test was based on 25 HDR images and 25 normal images classified by five users into nine classification categories. Where significant, the cover difference between HDR and normal images is given as the deviation from normal (difference). User × treatment interaction is given, first with all five users (interaction) and then with anomalous data from a single user removed for those classes that showed significant interaction. Classes that did not show significant user × treatment interaction were not run again with anomalous user data removed

visual acuity among users resulted in some seeing definition and color in dark areas where others could not. For example, a user with superior vision may see very well into dark pixels and therefore would not benefit much from having those pixels lightened, whereas a user with poor vision might see nothing in certain pixels unless they are lightened. We did not control for visual acuity and did not collect enough user data to test this conjecture; however, a difference in manual image classification by age group has been demonstrated (Booth et al. 2005). Among the small five-user group in this study, the user who classified the fewest pixels as shadow was the youngest, while the user who classified the fewest saturated pixels was the oldest, results which are consistent with previous findings.

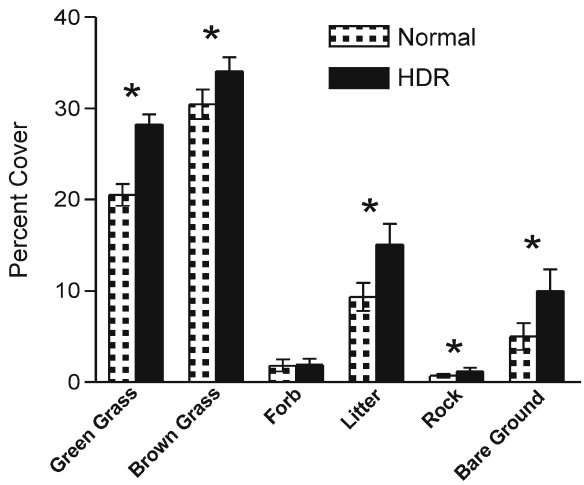

Fig. 4 Life form cover categories measured from 25 normal and 25 high dynamic range images by five users. *Error bars* show standard error of measurement. *Single asterisks* represent significant mean difference between image types ($P < 0.05$). The reduction of shadow in HDR images led to cover increases for most life forms

Across all users, classification of saturated areas in normal images (3.6% ± 2.9 SD) was lower than shadow (27.9% ± 7.8). We speculate there are two reasons for this. Saturated pixels in normal images were almost always surrounded by well-exposed pixels that made the context of the saturated pixels too clear to ignore (Fig. 1). For example, saturated pixels typically occurred on the shiny surfaces of grass leaf blades and were thus well-defined by the shape of the leaf. It is hard for a user to ignore shape during classification. In contrast, shadowed areas have a shape defined by the vegetative canopy, not by the darkened object(s) itself, and thus can include many cover types such as bare ground, litter, and smaller plants. The difference makes it much more likely that shadowed areas will confuse manual classification relative to saturated areas. Secondly, normal imagery luma distribution was heavily skewed towards the low end of the luma scale (Fig. 2), so there were many more dark than bright pixels to begin with.

All tests indicated improved feature separability with HDR imagery, thus demonstrating that this method provides a solution for shadowed imagery from a near-earth platform. The low sun angle and clear skies present during image acquisition and mixture of senesced and green vegetation within the plots resulted in deeper shadows and higher contrast than would be expected in images taken near midday during the growing season and thus represent the extreme end of shadowed imagery and a rigorous test of the benefits of HDR imagery.

Windy conditions prevalent in grass and shrub land ecosystems of the western USA make the acquisition of three digital images that can be perfectly overlaid no small feat. At the high resolutions that manual classification takes place, typically fractions of a millimeter, even small movements of the camera frame can cause image shift which manifests as a softly focused HDR image at high magnification, even when the software attempts to align the source images. Even using a rigid aluminum camera frame (Booth et al. 2004), we could not completely overcome the movement of the camera due to wind, and thus our HDR images were very slightly less crisp and sharp than the normal image. Results from the manual image analysis reflected this, with all users classifying more points as unknown in the HDR images relative to normal images (Fig. 3) and most verbally reporting noticeable reduction in HDR image clarity. One could naturally wait for windless conditions to acquire images, but across large swaths of western North America, one might be waiting a long time. Reinforcing the rigidity of the camera frame should assist in obtaining crisp HDR images, but this is likely a drawback to the method that will be difficult to completely eliminate. Additionally, grass and shrubs in the plot may move in the wind between shots, further introducing blur to the image in areas with tall vegetation. Short vegetation was much less affected by wind in our experiment.

HDR imagery from aerial platforms

Although the utility of photographing ground plots has been demonstrated and is immediately useful, images captured from aerial platforms offer greater potential for feature classification across landscapes. Shadows are no less of a problem in aerial images, and thus HDR images from an aerial perspective could potentially enhance classification accuracy as well as find wider use since aerial remote sensing is more widely practiced than near-earth remote sensing. However, similar to wind jarring a ground-based platform, an aerial platform presents the problem of a moving camera causing misalignment of images, leading to reduced-clarity HDR images. Potential solutions include stationary helicopter positioning over plots to increase image alignment precision, maximizing the ratio of image scale to image resolution to minimize the relative amount of blur due to misalignment of images, or utilizing multiple adjacent cameras firing at once, each at a different shutter speed. In the case of the latter, shutter speed is often dictated by movement of the aircraft and cannot be reduced without incurring added motion blur (Booth and Cox 2006), in which case the aperture must be adjusted (if possible), leading to depth-of-field differences that will reduce HDR image clarity (Brown 2006; HDRsoft 2007). Additionally, cameras must be aligned to one another with extremely high precision so as to ensure that each camera is capturing exactly the same field-of-view, otherwise the result is similar to a single camera taking three images while moving (unpublished data). Furthermore, using multiple camera lenses to photograph the same area could result in some degree of HDR image blur due to minor distortion differences among lenses. These are all significant obstacles to the generation of HDR imagery from an aerial platform, but the potential benefits of shadow-free aerial photography make this an area worthy of additional investigation. Future digital cameras may incorporate high dynamic range sensors which would capture more of the scene's dynamic range than current sensors and avoid the need for post-processing (Brown 2006).

Can a single image be made into a pseudo-HDR image by combining it with brightened and darkened versions of itself? This would eliminate blur due to multiple exposures from a moving camera, either on a fixed stand or from an aerial platform. Photomatix facilitates but does not

recommend this process, which must be carried out by manually brightening the TIF or RAW files to create the three base files used to generate the HDR image (Photomatix 2008). We generated HDR images in this way and found that, although color saturation improved in bright and dark areas, they lacked detail in bright and dark areas because the detail was not captured in these areas to begin with. In other words, lightening an area of the image that has no detail in it simply gives you a bright area with no detail in it. The software cannot create detail from nothing. Also, digital noise increased due to the brightening and darkening of the RAW image. The effect seemed more positive with ground than with aerial images, but this could be due to unique exposure and surface characteristics. We found that similar results could be obtained by simply adjusting the gamma and saturation levels in Photoshop. Thus, attempting to generate an HDR image from a single exposure seems to have, at best, limited value for classification enhancement.

Conclusions

The improvement in bare ground detection and general image clarity with HDR imagery suggests that many field applications would benefit from HDR image utilization. Collection of imagery from 1 to 3 m above ground for documenting natural resource condition is common practice (Cooper 1924; Wells 1971; Owens et al. 1985; Northrup et al. 1999; Paruelo et al. 2000; Louhaichi et al. 2001; Booth and Cox 2007). Instead of accepting shadowed imagery or shading the plot to reduce shadows (a difficult prospect under windy conditions), bracketed images of plots could simply be made into HDR images, eliminating the time required to transport and set up shading devices. In aerial applications where plot-shading is not applicable, HDR imagery could feasibly create images that have no darkened areas due to shadow, if certain technical obstacles can be overcome, thus improving the image quality and increasing analysis accuracy. HDR imagery has some limitations, and its benefits must be carefully weighed against its disadvantages, but it represents a new tool in the remote sensing toolbox that offers potential for increased analysis accuracy.

Acknowledgements Funding was provided by a grant to D.T. Booth from the Wyoming State Office of the Bureau of Land Management and by a grant to D.T. Booth from the Inter-Agency Powder River Aquatic Task Group. We thank Jessica Crowder, Pam Freeman, Larry Griffith, Carmen Kennedy, Gretchen Meyer, and Andrea Pettay for technical assistance, Robert Berryman for developing the C# pixel counting program and David Augustine for MRPP analysis. We also thank Andrea Laliberte and Sarah Swopes for reviewing the manuscript.

References

Anderson, G. L., Everitt, J. H., Escobar, D. E., Spencer, N. R., & Andrascik, R. J. (1996). Mapping leafy spruge (Euphorbia esula) infestations using aerial photography and geographic information systems. *Geocarto International, 11*, 81–89.

Bennett, L. T., Judd, T. S., & Adams, M. A. (2000). Close-range vertical photography for measuring cover changes in perennial grasslands. *Journal of Range Management, 53*, 634–641. doi:10.2307/4003159

Biondini, M. E., Mielke, P. W. Jr., & Berry, K. J. (1988). Data-dependent permutation techniques for the analysis of ecological data. *Vegetatio, 75*, 161–168.

Booth, D. T., & Cox, S. E. (2006). Very large scale aerial photography for rangeland monitoring. *Geocarto International, 21*(3), 27–34. doi:10.1080/10106040608542390

Booth, D. T., & Cox, S. E. (2007). Imaged-based monitoring to measure ecological change in rangeland. *Frontiers in Ecology and the Environment, 6*, 185–190.

Booth, D. T., & Tueller, P. T. (2003). Rangeland monitoring using remote sensing. *Journal of Arid Land Research and Management, 17*, 455–478. doi:10.1080/713936105

Booth, D. T., Cox, S. E., & Berryman, R. D. (2006). Point sampling digital imagery using 'SamplePoint'. *Environmental Monitoring and Assessment, 123*, 97–108. doi:10.1007/s10661-005-9164-7

Booth, D. T., Cox, S. E., & Johnson, D. E. (2005). Detection-threshold calibration and other factors influencing digital measurements of ground cover. *Rangeland Ecology and Management, 58*, 598–604. doi:10.2111/05-060R1.1

Booth, D. T., Cox, S. E., Louhaichi, M., & Johnson, D. E. (2004). Lightweight camera stand for close-to-earth remote sensing. *Journal of Range Management, 57*, 675–678. doi:10.2307/4004027

Bowman, D. M. J. S., Walsh, A., & Milne, D. J. (2001). Forest expansion and grassland contraction within a Eucalyptus savanna matrix between 1941 and 1994 at Litchfield National Park in the Australian monsoon tropics. *Global Ecology and Biogeography, 10*, 535–548. doi:10.1046/j.1466-822x.2001.00252.x

Brown, G. J. (2006). High dynamic range digital photography. *Royal Photographic Society Journal*, 428–431, November 2006

Clemmer, P. (2001). *Riparian area management—The use of aerial photography to manage riparian-wetland areas* (64 p.). Denver, CO: USDI Bureau of Land Management, Technical Reference 1737–10.

Cooper, W. S. (1924). An apparatus for photographic recording of quadrats. *Journal of Ecology, 12*, 317–321. doi:10.2307/2255254

Everitt, J. H., Yang, C., Racher, B. J., Britton, C. M., & Davis, M. R. (2001). Remote sensing of redberry juniper in the Texas rolling plains. *Journal of Range Management, 54*, 254–259. doi:10.2307/4003243

Fujita, T., Itaya, A., Miura, M., & Yamamoto, S. (2003). Canopy structure in a temperate old-growth evergreen forest analyzed by using aerial photographs. *Plant Ecology, 168*, 23–29. doi:10.1023/A:1024477227614

HDRsoft (2007). *Photomatix Pro 2.5 Users Manual* (28 p.). Montpellier, France: HDRsoft

Johnson, D. E., Vulfson, M., Louhaichi, M., & Harris, N. R. (2003). *VegMeasure v1.6 user's manual* (51p.). Corvallis, OR: Department of Rangeland Resources, Oregon State University

Lodriguss, J. (2003). Perceiving and recording light, range. *Photoshop for astrophotographers—A guide to basic digital correction and advanced enhancement techniques for astrophotos in Photoshop*. CD-ROM, URL: http://www.astropix.com/PFA/PFA.HTM

Louhaichi, M., Borman, M. M., & Johnson, D. E. (2001). Spatially located platform and aerial photography for documentation of grazing impacts on wheat. *Geocarto International, 16*, 63–68. doi:10.1080/10106040108542184

Naesset, E. (1998). Positional accuracy of boundaries between clearcuts and mature forest stands delineated by means of aerial photo interpretation. *Canadian Journal of Forest Research, 28*, 368–374. doi:10.119/cjfr-28-3-368

Nakashizuka, T., Katsuki, T., & Tanaka, H. (1995). Forest canopy structure analyzed by using aerial photographs. *Ecological Research, 10*, 13–18. doi:10.1007/BF02347651

Northrup, B. K., Brown, J. R., Dias, C. D., Skelly, W. C., & Radford, B. (1999). A technique for near-ground remote sensing of herbaceous vegetation in tropical woodlands. *The Rangeland Journal, 21*, 229–243. doi:10.1071/RJ9990229

Owens, M. K., Gardiner, H. G., & Norton, B. E. (1985). A photographic technique for repeated mapping of rangeland plant populations in permanent plots. *Journal of Range Management, 38*, 231–232. doi:10.2307/3898973

Paruelo, J. M., Laurenroth, W. K., & Roset, P. A. (2000). Estimating aboveground plant biomass using a photographic technique. *Journal of Range Management, 53*, 190–193. doi:10.2307/4003281

Photomatix (2008). Frequently Asked Questions Page, available at http://www.hdrsoft.com/support/faq_photomatix.html#raw. Accessed 08 September 2008.

Poynton, C. A. (1996). *A technical introduction to digital video* (320 p.). New York: Wiley.

Sawaya, K. E., Olmanson, L. G., Heinert, N. J., Brezonik, P. L., & Bauer, M. E. (2003). Extending satellite remote sensing to local scales: Land and water resource monitoring using high-resolution imagery. *Remote Sensing of Environment, 88*, 144–156. doi:10.1016/j.rse.2003.04.006

Stevenson, A., Baumgartner, R. E., & Schuman, G. E. (1984). *Detailed soil survey for the High Plains Grassland Research Station* (100 p.). Cheyenne, WY: Agricultural Research Service.

Wells, K. F. (1971). Measuring vegetation changes on fixed quadrats by vertical ground stereophotography. *Journal of Range Management, 24*, 233–236. doi:10.2307/3896780

Wittmann, F., Anhuf, D., & Junk, W. J. (2002). Tree species distribution and community structure of central Amazonian varzea forests by remote-sensing techniques. *Journal of Tropical Ecology, 18*, 805–820. doi:10.1017/S0266467402002523